Int. J. Heat Mass Transfer. Vol. 31, No. 1, pp. 79–90, 1988
Printed in Great Britain

0017–9310/88 $3.00 + 0.00
Pergamon Journals Ltd.

A semianalytical solution for heat-pipe effects near high-level nuclear waste packages buried in partially saturated geological media

CHRISTINE DOUGHTY and KARSTEN PRUESS

Earth Sciences Division, Lawrence Berkeley Laboratory, University of California, Berkeley, CA 94720, U.S.A.

(*Received* 25 *February* 1987 *and in final form* 10 *June* 1987)

Abstract—The emplacement of a strong heat source, such as a high-level nuclear waste package, in a partially saturated permeable medium will give rise to the development of a heat pipe. The present paper analyzes a simplified version of this problem that has a steady state solution, for radial geometry. The solution is obtained in semianalytical form, and is compared to the analogous solution for a linear heat pipe. Various applications are presented for porous as well as for fractured-porous media with different hydrologic properties. The parameters determining heat-pipe length and the question of whether the vicinity of the heat source dries up are discussed. The semianalytical solution is verified by numerical simulations that show the transient evolution from uniform initial conditions to the eventual steady state.

INTRODUCTION

HEAT PIPES are being widely applied in engineered heat-transfer systems, and various aspects of their behavior have been studied by many workers. The basic ingredients of a heat pipe are (1) a volatile fluid, and (2) a mechanism by which liquid and gas phases can flow in opposite directions. If heat is injected into such a system, the liquid phase will vaporize, causing pressurization of the gas phase and gas-phase flow away from the heat source. The vapor condenses in cooler regions away from the heat source, depositing its latent heat of vaporization there. This sets up a saturation profile, with liquid-phase saturations increasing away from the heat source. In engineered heat pipes incorporating porous media backflow of the liquid phase towards the heat source is effected by capillary forces. If noncondensible gases are present, they flow with the vapor away from the heat source and become concentrated in cooler regions. Heat pipes occur naturally on a large scale (kilometers) in a rare type of hydrothermal convection system known as vapor-dominated geothermal reservoirs [1–3]. In these systems a deep heat source of magmatic origin vaporizes water present in fractured porous rocks. The vapor rises in the fractures, and condenses at shallower depths on the cooler rock surfaces. The liquid condensate then flows back towards the heat source simply by the gravitational force. Effective heat conductivity in these systems can be several hundred W m^{-1} $°C^{-1}$, whereas heat conductivity of rocks is typically 1–3 W m^{-1} $°C^{-1}$.

Several workers have developed analytical and semianalytical solutions for the steady state behavior of one-dimensional heat pipes in homogeneous porous media, in conjunction with laboratory experiments [4–8]. All the formulations assume a linear one-dimensional geometry, and some include gravity.

In this paper we study a problem that arises in the context of nuclear waste isolation, namely, a heat pipe in one-dimensional radial (cylindrical) geometry. Numerical simulation studies by Pruess *et al.* [9] have shown that strong heat pipes can evolve near high-level nuclear waste packages buried in a partially saturated permeable material. This is of great practical significance, as it may have dramatic impacts on the waste package environment and design criteria (temperatures, presence or absence of moisture and air). The conditions that may be attained at some time following high-level waste emplacement are schematically depicted in Fig. 1. The waste package may

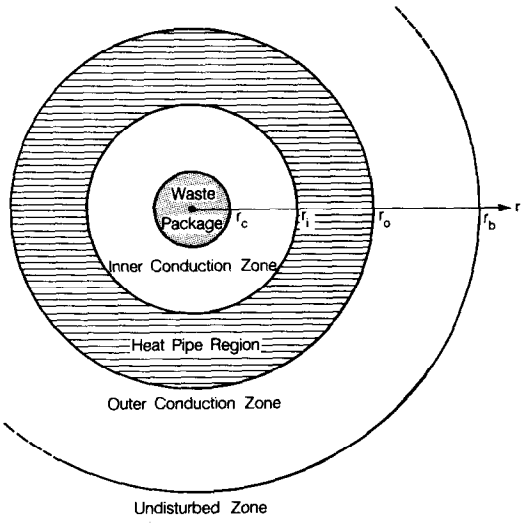

FIG. 1. Schematic of heat-transfer regimes in plane perpendicular to the axis of the waste packages (not to scale).

NOMENCLATURE

f	dimensionless capillary pressure, P_{cap}/P_{c0}
f'	derivative of f with respect to S
g	gravitational acceleration [m s^{-2}]
h_{vl}	vaporization enthalpy [J kg^{-1}]
K	thermal conductivity [W m^{-1} K^{-1}]
k	intrinsic permeability [m^2]
k_r	relative permeability
$\dot{m}$	mass flow rate per unit area [kg s^{-1} m^{-2}]
P	gas pressure [Pa]
P_a	partial pressure of air [Pa]
P_v	partial pressure of vapor [Pa]
P_l	liquid pressure [Pa]
P_{cap}	capillary pressure, $P_l - P_g$ [Pa]
P_{c0}	reference capillary pressure [Pa]
P_{sat}	saturation pressure [Pa]
Q	heat source strength [W m^{-1}]
q	heat flux, $Q/2\pi r$ in radial geometry [W m^{-2}]
R	gas constant for water, 461.52 J kg^{-1} K^{-1}
r	radial distance [m]
dr	radial mesh spacing [m]
Δr	heat-pipe length [m]
S_l	liquid saturation
S_{lr}	irreducible liquid saturation
S_{ls}	saturation at which liquid becomes fully mobile
S	scaled liquid saturation, $(S_l - S_{lr})/(S_{ls} - S_{lr})$
T	temperature [°C]
x_0	heat-pipe length in linear geometry [m]
Y	air mole fraction.

Greek symbols

β	ratio of kinematic viscosity for liquid and vapor
δ	dimensionless distance, equation (A11)
λ	parameter in characteristic curves
ν	kinematic viscosity [m^2 s^{-1}]
ρ	density [kg m^{-3}]
σ	vapor–liquid interfacial tension [N m^{-1}]
ϕ	porosity
ψ	function governing heat-pipe length
ω	dimensionless heat source strength, equation (A12).

Subscripts

a	air
b	outer boundary of system
c	waste canister
f	fracture
g	gaseous phase
i	inner boundary of heat pipe
l	liquid phase
o	outer boundary of heat pipe
v	vapor.

be surrounded by a dried zone, in which heat transfer occurs primarily by conduction. At larger distances a heat-pipe region may be present, beyond which there is another zone with predominantly conductive heat transfer, where temperatures are too low for significant evaporation and heat-pipe effects to occur. Depending on the properties of the permeable medium and the rate of heat input, the heat-pipe region can extend all the way to the heat source, or it can be extremely short.

For the problem of geologic disposal of high-level nuclear waste, heat-pipe conditions will be of a transient nature, as heat is transferred from a localized source at a time-varying rate into a large (essentially infinite) rock mass. The problem addressed in this paper has been simplified by assuming that (1) the rate of heat generation is constant, independent of time; and (2) time-independent boundary conditions are posed at a finite distance from the heat source. With these two simplifications the system will attain steady state conditions, for which an approximate semianalytical solution can be obtained. Additional approximations will be introduced during the theoretical formulation below. The approximations made in the derivation of the semianalytical solution are discussed and are found to be applicable only when the permeability of the medium is low. However, our solution will be useful for verifying complex numerical simulators even under conditions where certain approximations, such as neglect of gravity effects, are not justified. After showing several examples of the semianalytical solution for different geological conditions, we report fully-transient numerical simulations of the heat-pipe process near a cylindrical heat source, to verify the accuracy of the assumptions made for the semianalytical solution and to put the semianalytical steady state solution in context.

THEORETICAL FORMULATION

Present design considerations assume nuclear wastes to be packaged in cylindrical canisters of about 4.5 m length and 0.5 m diameter [10]. This shape gives rise to a two-dimensional cylindrically symmetric heat flow pattern around each canister. To simplify the analysis, we eliminate end effects by considering a heat source as an infinitely long string of cylindrical waste packages. Further, by neglecting gravity effects and assuming that boundary conditions depend only on radial distance r from the symmetry axis, fluid and heat flow will possess one-dimensional radial symmetry. The condition under which gravity effects can

be neglected is discussed in the Appendix. For time-independent boundary conditions, the system will attain a steady state.

Under steady state conditions, three domains with different heat-transfer mechanisms are presumed to exist in the porous medium around the heat source (see Fig. 1). Beyond some distance r_b the influence of the heat source is not felt and the system is undisturbed. The outermost domain of the disturbed zone is a liquid water/air domain. Temperatures are below the saturation temperature so little evaporation occurs, leaving gas-phase pressures nearly uniform, resulting in little mass flow and conduction-dominated heat flow. The middle domain is a two-phase liquid/vapor zone at the saturation temperature, the heat-pipe region, where heat flow is primarily convective. Air is purged from this region by the vapor flow away from the heat source. The innermost domain is a vapor zone in which little mass flow occurs and heat flow is conduction dominated. The present approach is to start at r_b and work inward to determine the conditions near the canister, specifically whether the inner vapor zone is present. The variables used to describe the state of the system are gas-phase pressure P, temperature T, air partial pressure P_a, and liquid saturation S_l. It is also convenient to define a scaled liquid saturation S, given by $S = (S_l - S_{lr})/(S_{ls} - S_{lr})$, where S_{lr} is the irreducible liquid saturation, and S_{ls} is the saturation at which liquid relative permeability becomes equal to 1.

The pressure, temperature, and saturation conditions are assumed fixed at a radial distance of r_b. These boundary conditions are denoted P_b, T_b, and S_{lb}, respectively. The specification of P_b and T_b fixes P_{ab}, air partial pressure at r_b, through the saturation curve. The scaled liquid saturation at the boundary is given by $S_b = (S_{lb} - S_{lr})/(S_{ls} - S_{lr})$. A constant heat source of strength Q is prescribed at the waste canister radius r_c. For steady state conditions and radial geometry this leads to a heat flux given by $q(r) = Q/2\pi r$ for all radial distances r.

Outer conduction zone

In the outer conduction zone (see Fig. 1) total pressure and saturation are assumed to be equal to the boundary values. Heat flow is primarily conductive, so that the temperature at a distance r can be approximately expressed as

$$T(r) = T_b + \frac{Q}{2\pi K_b} \ln\left(\frac{r_b}{r}\right) \tag{1}$$

where K_b is the thermal conductivity of the medium at a saturation S_{lb}. The saturation dependence of thermal conductivity for geologic media has been studied by Somerton *et al.* [11, 12]. The gas phase in the outer conduction zone is a mixture of air and vapor. Air partial pressure is

$$P_a = P_b - P_v \tag{2}$$

with vapor pressure P_v given by the Kelvin equation

$$P_v(T, S) = P_{sat}(T) \cdot \exp\left(\frac{P_{cap}(S)}{\rho_l R(T + 273.15)}\right) \tag{3}$$

where P_{sat} is saturation pressure, P_{cap} is capillary pressure (negative), ρ_l is liquid density, and R is the gas constant for water. For weak or moderate capillary pressures, vapor pressure lowering effects are small, and the exponential factor can be replaced by 1. (A 1% lowering of vapor pressure requires a capillary pressure of about $P_{cap} = -13$ bar.)

Equation (1) shows that T steadily increases as r decreases; equation (3) indicates a corresponding increase in P_v, while a concurrent decrease in P_a follows from equation (2). When P_v becomes equal to the total pressure P_b (and $P_a = 0$), heat-pipe conditions develop. The temperature T_o at which this occurs can be obtained implicitly from equation (3)

$$P_{sat}(T_o) \cdot \exp\left(\frac{P_{cap}(S_b)}{\rho_l R(T_o + 273.15)}\right) = P_b. \tag{4}$$

The outer boundary of the heat pipe, r_o, can be obtained by solving equation (1) for $T(r_o) = T_o$. At r_o, we have $P_o = P_b$, $P_{a0} = 0$, and $S_o = S_b$. The variation of saturation with radial distance between r_o and the inner boundary of the heat pipe, r_i, is derived in the Appendix. The parameter r_i is determined from the condition $S_i \equiv S(r_i) = 0$.

Inner conduction zone

If $r_i < r_c$ then two-phase conditions extend all the way to the heat source, and the inner conduction zone is absent. If $r_i > r_c$ then a single-phase vapor zone, in which heat transfer is conduction dominated, develops around the heat source. The value of T_c can then be calculated from

$$T_c = T_i + \frac{Q}{2\pi K_v} \ln\left(\frac{r_i}{r_c}\right) \tag{5}$$

where T_i is the temperature at the inner boundary of the heat pipe, and K_v is the thermal conductivity of the vapor-saturated porous medium. Because K_v is small, and Q can be large, T_c can be much higher than T_i. As well as causing a large increase in T_c, the formation of a vapor zone around the heat source inhibits chemical reactions that are facilitated by the presence of liquid water, such as corrosion of the canister.

Heat-pipe region

Fluid and heat flow in the heat-pipe region are considered in the Appendix. By integrating equation (A15), the saturation profile along the heat pipe can be obtained as an implicit function of radius

$$\omega \int_{r_o}^{r} d\delta = \omega\delta(r) = \int_{S_b}^{S(r)} \frac{-f'}{\dfrac{1}{k_{rv}} + \dfrac{\beta}{k_{rl}}} dS. \tag{6}$$

Equation (6) is of the same form as Udell's equation (24) [8] for linear geometry. For moderate heat flux, temperature variations along the heat pipe are small, and the integrand in equation (6) is primarily a function of S. It can be integrated numerically for given capillary pressure and relative permeability functions. In the examples below we have integrated equation (6) using the cautious adaptive romberg extrapolation (CADRE) numerical integration algorithm [13]. The inner boundary of the heat pipe, r_i, can be found by integrating equation (6) to $S(r_i) = 0$

$$\omega\delta(r_i) = \int_{S_b}^{0} \frac{-f'}{\dfrac{1}{k_{rv}} + \dfrac{\beta}{k_{rl}}} \mathrm{d}S \equiv -\psi(\beta, S_b). \tag{7}$$

The function $\psi(\beta, S_b)$, which governs total heat-pipe length is shown in Fig. 2 for the P_{cap}, k_{rv}, and k_{rl} functions given in Table 3, case A and several values of S_{lb}. Substituting the definitions for ω and δ into equation (7) yields r_i:

$$r_i = r_o \exp\left[\frac{2\pi\psi(\beta, S_b)h_{vl}P_{c0}k}{Qv_v}\right] \tag{8}$$

where h_{vl} is the latent heat of evaporation of water, P_{c0} is a (negative) reference capillary pressure, k is intrinsic permeability, and v_v is vapor kinematic viscosity.

The pressure profile in the heat pipe can be similarly obtained by noting that

$$\frac{\mathrm{d}P_v}{\mathrm{d}S} = \frac{\dfrac{\mathrm{d}P_v}{\mathrm{d}r}}{\dfrac{\mathrm{d}S}{\mathrm{d}\delta}\cdot\dfrac{\mathrm{d}\delta}{\mathrm{d}r}} \tag{9}$$

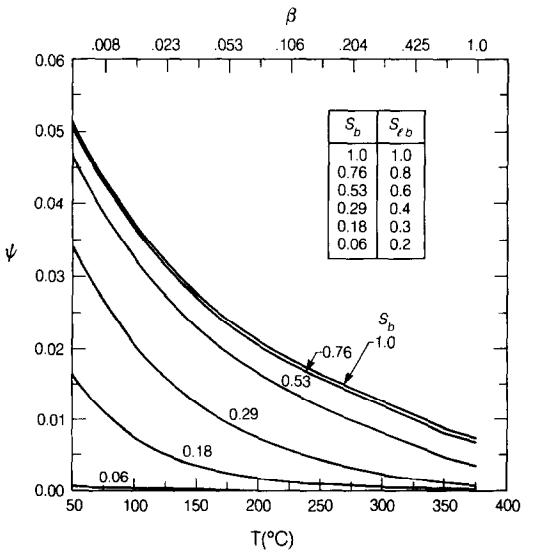

FIG. 2. The function $\psi(\beta, S_b)$ for a range of temperatures and saturation boundary conditions, calculated using characteristic curves given in Table 3, case A. The values of S_{lb} are calculated from $S_{lb} = S_b(S_{ls} - S_{lr}) + S_{lr}$, with $S_{lr} = 0.15$ and $S_{ls} = 1.0$.

and using equation (A15) for $\mathrm{d}S/\mathrm{d}\delta$, equation (A2) for $\mathrm{d}P_v/\mathrm{d}r$, and differentiating equation (A11) to obtain $\mathrm{d}\delta/\mathrm{d}r$. Finally, equation (3) can be solved implicitly to obtain temperatures from pressures.

The condition under which the vicinity of the heat source will dry up is $r_c < r_i$. From equations (1) and (8) this can be written, neglecting vapor pressure lowering, as

$$\exp\left\{\frac{2\pi}{Q}\left[K_b(T_{sat}(P_b) - T_b) - \frac{\psi h_{vl}P_{c0}k}{v_v}\right]\right\} < \frac{r_b}{r_c}. \tag{10}$$

Because $T_{sat}(P_b) > T_b$ and $P_{c0} < 0$, both terms in the exponential function are positive. It is seen that fulfillment of inequality (10), i.e. dry-up of the heat source, is facilitated by large heat flux Q and small permeability k.

COMPARISON WITH LINEAR GEOMETRY CASE

For the linear geometry case with $S_b = 1$, Udell [8] obtains an expression for the length of the heat pipe x_0 given by

$$x_0 = \frac{-\psi(\beta, 1)h_{vl}P_{c0}k}{qv_v}. \tag{11}$$

Taking the heat flux q in the radial flow case at the inner end of the heat pipe, $q = Q/2\pi r_i$, equation (8) can be written as

$$r_i = r_o \mathrm{e}^{-x_0/r_i}. \tag{12}$$

The heat-pipe length is

$$\Delta r = r_o - r_i = r_i(\mathrm{e}^{x_0/r_i} - 1). \tag{13}$$

Expanding the exponential, this becomes

$$\Delta r = x_0\left(1 + \frac{x_0}{2r_i} + \frac{x_0^2}{6r_i^2} + \ldots\right) \tag{14}$$

showing that heat-pipe length in radial geometry can be substantially larger than in linear geometry. For heat pipes far removed from the canister (r_i large) or short heat pipes (x_0 small), $(x_0/r_i) \to 0$, linear geometry is being approached, and therefore $\Delta r \to x_0$.

EXAMPLES

We have applied the above formulation to calculate steady state thermo-hydrologic conditions near a cylindrical heat source emplaced in a partially saturated porous medium for a variety of problem parameters (see Tables 1–3). The heat source radius and strength are $r_c = 0.2$ m and $Q = 500$ W m^{-1}, respectively. At the outer boundary $r_b = 10$ m, ambient conditions of $T_b = 26°C$, $P_b = 1$ bar, and $S_{lb} = 0.8$ prevail. In cases A–C permeability and porosity are 10^{-12} m^2 and 0.4, respectively, which represents a laboratory sand pack. In cases D–F we take $k = 32.6 \times 10^{-18}$ m^2 and $\phi = 0.108$, as has been suggested for Yucca Mountain tuffs [10]. From equation (7) we see that the length of

Table 1. Material properties (at $T = 101°C$)

$\beta = 0.0142$	
$v_v = 18.9 \times 10^{-6}\ m^2\ s^{-1}$	$K_b = 1.07\ W\ m^{-1}\ °C^{-1}$
$h_{vl} = 2.257 \times 10^6\ J\ kg^{-1}$	$K_v = 0.582\ W\ m^{-1}\ °C^{-1}$
$\sigma = 0.05878\ N\ m^{-1}$	

Table 2. Boundary conditions

At $r_b = 10$ m	$S_{lb} = 0.8$
	$P_b = 1$ bar
	$T_b = 26°C$
At $r_c = 0.2$ m	$Q = 500\ W\ m^{-1}$

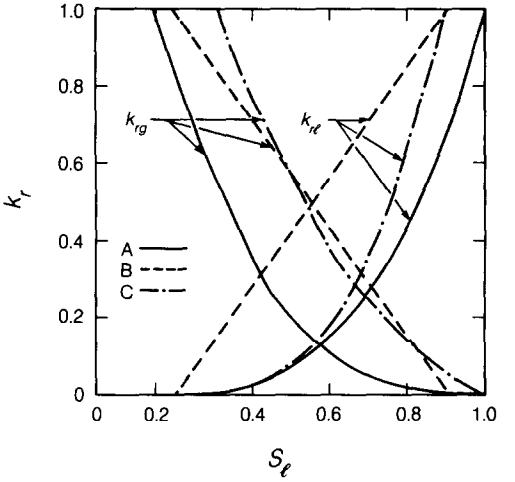

FIG. 3. Relative permeability curves for cases A–C.

the heat pipe depends strongly on the relative permeability functions, k_{rv} and k_{rl}, so the different cases examine the effect of various functional forms for relative permeability. The relative permeability curves for cases A–C are shown in Fig. 3, while those for cases D–F are shown in Fig. 4. The resulting saturation, pressure, temperature, and composition profiles are given in Figs. 5–8; for convenience we have plotted air mole fraction $Y = P_a/P$ rather than partial pressure P_a.

The characteristic curves for case A have been used for laboratory studies using packed sand cores [8, 14–16]. Case B uses the same capillary pressure function, but a linear rather than cubic saturation dependence for relative permeabilities, as has been suggested by other workers [5, 7]. The effect of using either cubic or linear relative permeability curves is clearly seen by comparing Figs. 5 and 6. In Fig. 5 (case A, cubic relative permeabilities) the heat pipe is short enough

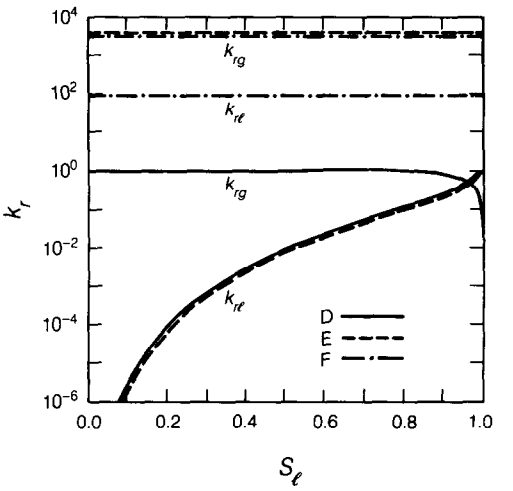

FIG. 4. Relative permeability curves for cases D–F.

Table 3. Characteristic curves for relative permeability and capillary pressure dependence on saturation

Case	Capillary pressure	Relative permeability
A†	$P_{cap} = P_{c0} f$ $P_{c0} = -\sigma(\phi/k)^{1/2}$ $f = a(1-S)+b(1-S)^2+c(1-S)^3$ $a = 1.417,\ b = -2.12,\ c = 1.263$	$k_{rl} = S^3$ $k_{rv} = (1-S)^3$ $S_{lr} = 0.15,\ S_{ls} = 1.0$
B	Same as A	$k_{rl} = S$ $k_{rv} = 1-S$ $S_{lr} = 0.2,\ S_{ls} = 0.895$
C	Same as A	$k_{rl} = S^3$ $k_{rv} = a+bS+cS^2$ $a = 1.259,\ b = -1.7615,\ c = 0.5089$ $S_{lr} = 0.2,\ S_{ls} = 0.895$
D‡	$P_{cap} = P_{c0} f$ $P_{c0} = -13.93$ bar $f = (S^{-1/\lambda}-1)^{1-\lambda}$	$k_{rl} = \sqrt{S}[1-(1-S^{1/\lambda})^\lambda]^2$ $k_{rv} = 1-k_{rl}$ $S_{lr} = 9.6 \times 10^{-4},\ S_{ls} = 1.0,\ \lambda = 0.45$
E	Same as D	$k_{rl} = \sqrt{S}[1-(1-S^{1/\lambda})^\lambda]^2$ $k_{rv} = 3067$ $S_{lr} = 9.6 \times 10^{-4},\ S_{ls} = 1.0,\ \lambda = 0.45$
F	Same as D	$k_{rl} = 90.65$ $k_{rv} = 2976$

† After Udell [8]. ‡ After Hayden *et al.* [10].

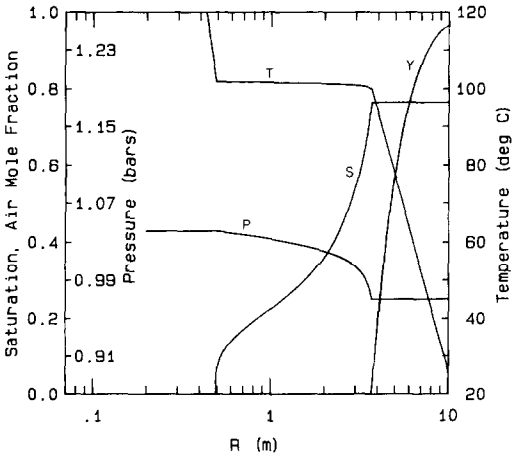

FIG. 5. Analytical solution for scaled-saturation, pressure, temperature, and air-mole-fraction profiles, for case A. The temperature at the canister, T_c, is 225°C.

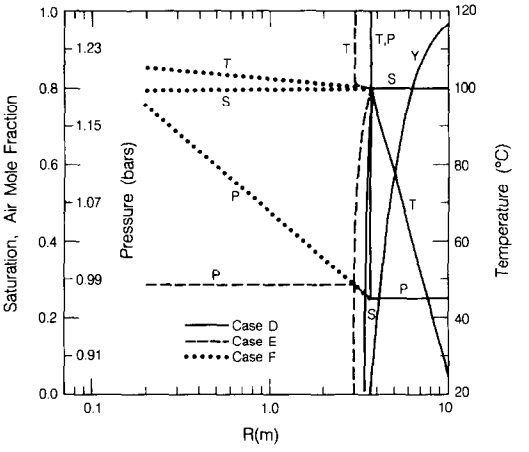

FIG. 8. Analytical solution for scaled-saturation, pressure, temperature, and air-mole-fraction profiles for cases D–F.

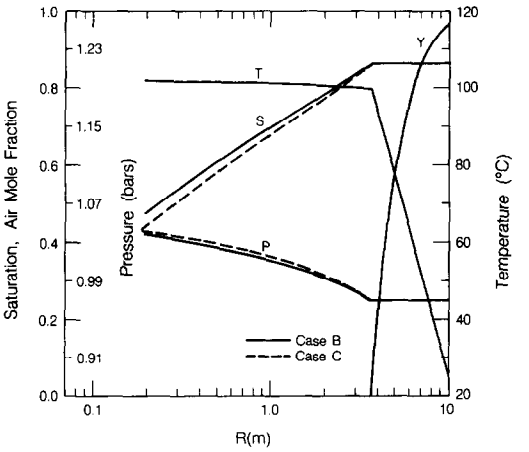

FIG. 6. Analytical solution for scaled-saturation, pressure, temperature, and air-mole-fraction profiles for cases B and C, where $Q = 500$ W m^{-1}.

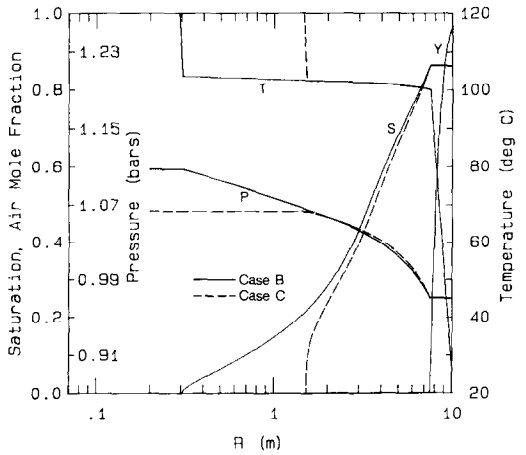

FIG. 7. Analytical solution for scaled-saturation, pressure, temperature, and air-mole-fraction profiles for cases B and C, when $Q = 1750$ W m^{-1}.

so that a vapor zone forms around the canister, leading to high temperatures at the canister. In Fig. 6 (case B, linear relative permeabilities) the saturation decline towards the canister is more gradual, yielding a longer heat pipe. At the canister radius, there is still liquid present, so temperature remains near the saturation temperature. The effect of relative permeability functions can be predicted qualitatively by examining equation (7) and the relative permeability curves for cases A and B (Fig. 3). The cubic relative permeabilities (case A) are smaller than the linear ones (case B) over the entire range of liquid saturation where both phases are mobile. Thus the denominator of the integrand in equation (7) is consistently bigger for the cubic functions, leading to a smaller value of ψ, and consequently a shorter heat pipe.

The relative permeability curves of cases A and B are commonly used in the petroleum literature, but their applicability to two-phase water flow is less well established. Case C uses relative permeabilities as measured in laboratory experiments on liquid–vapor water flow [17]. The saturation profile for case C is similar to that for case B (Fig. 6); liquid saturation remains large and no vapor zone forms at the canister. A careful examination of equation (7) and Fig. 3 shows why this is so. The magnitude of the integrand in equation (7) is dominated by the smaller of the two relative permeabilities. Figure 3 shows that for large liquid saturations, vapor relative permeability is smaller and therefore the controlling factor in equation (7). Further, k_{rv} values for cases B and C are similar for large S_l, and much larger than k_{rv} for case A. Thus the saturation profiles for cases B and C are similar to each other (Fig. 6), but different from that for case A (Fig. 5).

For small liquid saturations, k_{rl} is smaller than k_{rv}, so k_{rl} becomes the controlling factor in equation (7). Since the k_{rl} curves are different for cases B and C, one would expect the resulting saturation profiles to differ for small values of S. Figure 7 shows the heat-

pipe conditions for cases B and C with a larger heat flux, $Q = 1750$ W m^{-1}. As predicted, the saturation profiles diverge significantly only when S becomes small.

Case D uses characteristic curves [18] that have been suggested for the rock matrix of the candidate nuclear waste repository site at Yucca Mountain, Nevada [9, 10]. The saturation and temperature profiles (Fig. 8) show that the heat pipe is extremely short and there is no isothermal two-phase zone separating the inner and outer conduction zones. This result is supported by equation (8), which shows that heat-pipe length depends exponentially on absolute permeability k, which is much smaller for case D (32.6×10^{-18} m^2) than for cases A–C (10^{-12} m^2). It should be pointed out that the potential repository horizon at Yucca Mountain is highly fractured [10], and the case D parameters neglecting fracture effects are considered unrealistic.

For the important case of a fractured-porous medium, Pruess *et al.* [9] developed an effective continuum approximation, in which rock matrix and fractures are assumed to be in (approximate) thermodynamic equilibrium locally. Under conditions where this approximation is applicable, discussed in ref. [9], it is not necessary to explicitly consider 'interporosity' flow between matrix and fractures. Fluid and heat flow can be approximately described as occurring in a single porous continuum with effective hydrologic properties. Essentially, fracture effects are represented by suitably modified relative permeability functions. Effects of large fracture permeabilities are approximated by allowing relative permeability to become large. Following Pruess *et al.* [9] we have considered two effective continuum cases, E and F, which differ with respect to assumed liquid-phase mobility in the fractures. Case E makes the conventional assumption that at ambient conditions of $S_{lb} = 80\%$, corresponding to a capillary pressure of $P_{cap} = -10.92$ bar, the fractures are drained of liquid so that the large fracture permeability is available only for gas-phase flow. Fracture flow effects can then be simply represented by assigning a large constant relative permeability $k_{rv} = k_f/k$ to the gas phase, where k_f is average fracture permeability in the continuum sense. For an assumed $k_f = 10^{-13}$ m^2, we have $k_{rv} = 3067$ (see Table 3 and ref. [9]). Alternatively it appears possible that a finite liquid-phase mobility may be present in fractures the bulk volume of which has been drained, because of liquid held on the fracture surfaces by phase adsorption forces, or by capillary effects from surface roughness. Case F uses the relative permeability parameters proposed by Pruess *et al.* [9] to represent mobility of both gas and liquid phases in the fractures. Figure 8 compares the effective continuum calculations with the results for the unfractured case (case D), and shows that allowance for gas flow in the fractures (case E) causes a moderate increase in heat-pipe length, whereas additional allowance for liquid flow in the fractures (case F) gives dramatic effects. In the latter case the heat pipe extends all the way to the heat source. With no dried conductive zone present, temperatures remain constrained near 100°C. For case F the constant relative permeabilities allow direct integration of equation (7)

Table 4. Non-dimensional heat flux ω for each case; values of $\omega > 1$ signify that gravity effects are small

Case	Q	ω
A, B, C	500	0.2
B, C	1750	0.7
D, E	500	641.0
F	500	7.1†

† $k_{rl} \cdot k$ used instead of k.

$$\omega\delta(r_i) = \frac{f(S_b) - f(0)}{\dfrac{1}{k_{rv}} + \dfrac{\beta}{k_{rl}}}. \tag{15}$$

Table 4 shows the values of ω for each case, to illustrate the importance of gravity effects. For the high-permeability cases A–C, $\omega < 1$, so gravity effects may be important. The present analysis is therefore only valid for horizontal flow, i.e. for emplacement conditions where the axis of the cylindrical canister is vertical, and where host formation permeability is significantly smaller in the vertical than in the horizontal direction. In contrast, for cases D–F, $\omega > 1$ so the present analysis neglecting gravity can be applied to all flow directions.

COMPARISON WITH NUMERICAL SIMULATIONS

The numerical model TOUGH [19, 20] has been used to study the transient development of heat pipes, and to examine the assumptions made for the analytical solutions presented above for the steady state. TOUGH (transport of unsaturated groundwater and heat) calculates the two-phase flow of air and water in gaseous and liquid phases together with heat flow in a fully coupled way. The governing equations account for gaseous diffusion and Darcy flow with relative permeability and capillary pressure effects. Vaporization and condensation with latent heat effects along with conductive and convective heat flow are included in the energy balance. Water, air, and rock are assumed to be in local thermodynamic equilibrium at all times. The flow domain can include liquid, gaseous, and two-phase regions. Material properties vary with temperature and pressure in a realistic way. TOUGH uses an integral finite difference method that is applicable for one-, two-, or three-dimensional flow problems in porous or fractured porous media. The governing mass- and energy-balance equations are strongly nonlinear and are solved completely simultaneously, using Newton–Raphson iteration.

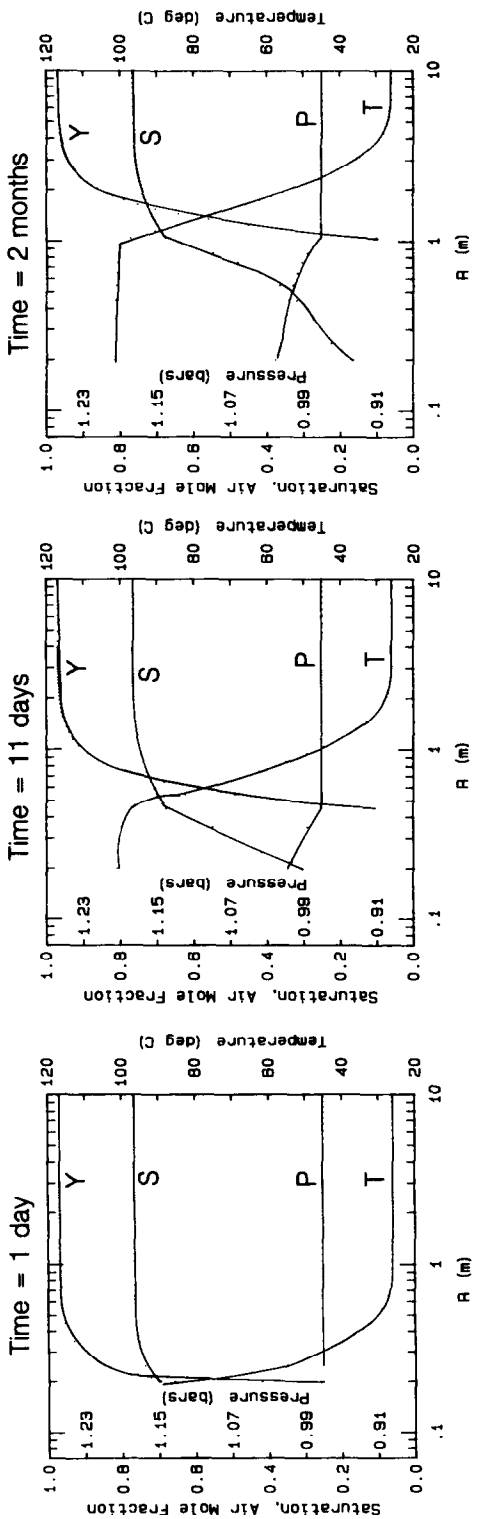

FIG. 9. Numerically-simulated scaled-saturation, pressure, temperature, and air-mole-fraction profiles at various times. For steady state conditions, numerical and analytical solutions are both shown.

A one-dimensional radial calculational mesh with 50 elements is used to calculate $S(r)$, $P(r)$, $P_a(r)$, and $T(r)$ around a heat source for case A (see Tables 1–3). The parameters in the left-hand column of Table 1 vary with temperature in TOUGH, but are considered constants for the analytical solution. Because the heat pipe is nearly isothermal, this difference is not significant [21]. Further, because the analytical solution does not consider air in the heat-pipe region, we set the coefficient of binary diffusion to zero in the simulations. The two innermost elements of the mesh, $0 < r < 0.2$ m, include the heat source, with strength $Q = 500$ W m^{-1}. The mesh has a spacing of $dr = 0.1$ m where heat-pipe effects are expected (0.2–4 m), and $dr = 0.6$ m for the outer conduction zone (4–10 m). Initial conditions are everywhere equal to P_b, T_b, and S_{lb}.

A calculation to steady state takes 300 time steps and requires 2.7 min of CPU time on a Cray X-MP. Figure 9 shows the transient development of the heat pipe, with the analytical solution superimposed on the final frame, which shows steady state conditions. The agreement is good. In the numerical simulation liquid saturation shows some variation in the outer conduction region, suggesting a weak heat-pipe (liquid–vapor counterflow) process in the region with $T < T_{sat}(P_b)$. However, the good agreement of the numerical and analytical temperature profiles indicates that conduction is the dominant heat-transfer mechanism. The small temperature variation in the heat-pipe region justifies the neglect of conduction there, whereas the linear temperature profile in the inner conduction zone validates the conduction-only assumption made for that region.

The assumption of constant saturation in the outer conduction region results in a difference of about 0.1 between the analytical and simulated values of S at r_o. This difference is the source of the discrepancy between the analytical and simulated pressure profiles in the heat-pipe region, and the slight difference in saturation profiles for $S > 0.2$. If the analytical saturation at r_o is arbitrarily set to match the numerically simulated value there, then the analytical pressure profile matches the simulated one closely, and the analytical and simulated saturation profiles for $S > 0.2$ agree well. By using a finer mesh, the numerically simulated saturation profile matches the analytical one closely for $S < 0.2$, near r_i. Figure 10 shows the analytical solution and the numerically simulated results for a mesh with 132 elements, with finest resolution, $dr = 0.01$ m, around r_i. This simulation would be expensive if it began with uniform initial conditions as the previous simulation did; instead it begins with the final conditions simulated by the 50 element mesh. This progression from coarse to fine calculational mesh provides an efficient way to use numerical models to study analytical solutions. Also shown in Fig. 10 are the results of a simulation including binary diffusion. Departures from the no-binary-diffusion simulation are small, and limited to the vicinity of r_o.

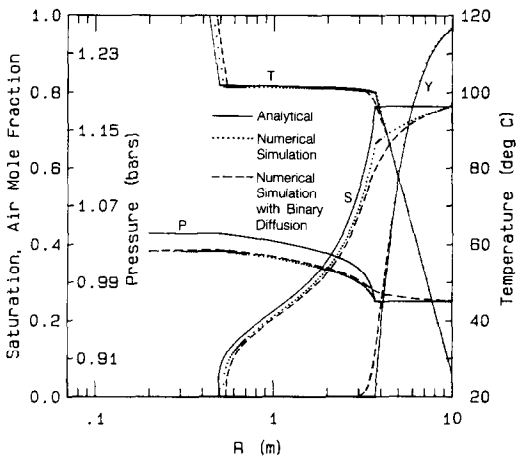

FIG. 10. Steady state profiles simulated numerically using a fine mesh, compared with the analytical solution. Profiles for a simulation including binary diffusion are also shown.

For the linear geometry case the treatment is similar, and an equally good match was found between the numerically simulated results [20, 21] and the analytical solution [8, 22]. The linear-geometry verification is especially valuable for two reasons. First, laboratory experiments have been done to validate the linear-geometry analytical solution [8], thus providing experimental validation of the numerical model, making it a more reliable check of the radial-geometry solution. Second, extensions of the linear-geometry analytical solution have been developed [22, 23] that include conduction and gas-phase diffusion as well as convection and phase change. These solutions verify the existence of distinct conduction- and convection-dominated zones, as postulated for the present work, and show the range of conditions for which this assumption is valid.

CONCLUSIONS

Under steady state conditions three domains may exist around a cylindrical heat source emplaced in a partially saturated geological medium: a vapor-phase inner conduction zone, a two-phase heat-pipe region, and a liquid water/air outer conduction zone. A heuristic model of mass and energy transport has been used to develop approximate analytical solutions for pressure, temperature, and liquid saturation profiles around the heat source. The accuracy of these solutions has been verified by numerical simulations. The solutions offer a convenient means for addressing the important question of whether the vicinity of the heat source will dry up. In addition, the semianalytical solution offers a convenient means for evaluating the accuracy of numerical simulation codes.

The extent of the heat-pipe region can be much greater for radial geometry than for linear geometry, a consequence of the decrease in flow rate per unit

area that occurs with radial distance. Because fluxes diminish with radial distance, smaller pressure gradients are needed to drive them. This leads to a smaller capillary pressure gradient, resulting in a smaller saturation gradient and a longer two-phase zone.

The characteristic curves for relative permeability and capillary pressure also have a strong influence on the extent of the heat pipe. Fractured/porous media provide conditions that are favorable for heat-pipe development, namely, large permeability in the fractures and strong capillary effects in the porous matrix.

Future work plans include a study of the transient pressure, temperature, and saturation profiles that develop following emplacement of a heat source.

Acknowledgements—The careful review of this work by Y. W. Tsang and J. S. Y. Wang is gratefully appreciated. This work was supported, in part, by the Waste Management Branch, Division of Radiation Programs and Earth Sciences, Office of Nuclear Regulatory Research, U.S. Nuclear Regulatory Commission; and the U.S. Department of Energy under Contract No. DE-AC03-76SF00098.

REFERENCES

1. D. E. White, L. J. P. Muffler and A. H. Truesdell, Vapor-dominated hydrothermal systems compared with hot-water systems, *Econ. Geol.* **66**(1), 75–97 (1971).
2. G. Schubert and J. M. Straus, Steam–water counterflow in porous media, *J. Geophys. Res.* **84**(B4), 1621–1628 (1979).
3. K. Pruess, A quantitative model of vapor dominated geothermal reservoirs as heat pipes in fractured porous rock, *Trans. Geoth. Res. Coun.* **9**(II), 353–361 (1985).
4. V. Dhir and I. Catton, Dryout heat fluxes for inductively heated particulate beds, *J. Heat Transfer* **99**, 250–256 (1977).
5. H. C. Hardee and R. H. Nilson, Natural convection in porous media with heat generation, *Nucl. Sci. Engng* **63**, 119–132 (1977).
6. Y. Ogniewicz and C. L. Tien, Porous heat pipe. In *Heat Transfer, Thermal Control, and Heat Pipes* (Edited by W. B. Olstad), Vol. 70, *Progress in Astronautics and Aeronautics* (Series Editor M. Summerfield), pp. 329–345. AIAA, New York. Presented as paper 79-1093, AIAA 14th Thermophysics Conf., Orlando, Florida, June (1979).
7. H. H. Bau and K. E. Torrance, Boiling in low-permeability porous materials, *Int. J. Heat Mass Transfer* **25**(1), 45–55 (1982).
8. K. S. Udell, Heat transfer in porous media considering phase change and capillarity—the heat pipe effect, *Int. J. Heat Mass Transfer* **28**(2), 485–495 (1985).
9. K. Pruess, Y. W. Tsang and J. S. Y. Wang, Modeling of strongly heat driven flow in partially saturated fractured porous media. In *Memoirs, International Association of Hydrogeologists*, Vol. XVII, pp. 486–497 (1985).
10. N. K. Hayden, J. K. Johnstone and R. R. Peters, Parameters and material properties for hydrologic modeling of the Topopah Spring unit, Memo to distribution, Sandia National Laboratories, 27 September (1983).
11. W. H. Somerton, J. A. Keese and S. L. Chu, Thermal behavior of unconsolidated oil sands, Paper SPE-4506, presented at 48th Annual Fall Meeting of the Society of Petroleum Engineers, Las Vegas (1973).
12. W. H. Somerton, A. H. El-Shaarani and S. M. Mobarak, High temperature behavior of rocks associated with geothermal type reservoirs, Paper SPE-4897, presented at 44th Annual California Regional Meeting of the Society of Petroleum Engineers, San Francisco (1974).
13. *IMSL Library Edition 9 Reference Manual*, Chap. D. IMSL, Houston (1982).
14. I. Fatt and W. A. Klikoff, Effect of fractional wettability on multiphase flow through porous media, AIME Technical Note #2043, *AIME Trans.* **216**, 246 (1959).
15. M. C. Leverett, Capillary behavior in porous solids, *AIME Trans.* **142**, 152–169 (1941).
16. M. R. J. Wyllie, Relative permeability. In *Petroleum Production Handbook* (Edited by T. C. Frick), Vol. 2, Chap. 25. McGraw-Hill, New York (1962).
17. A. K. Verma, K. Pruess, C. F. Tsang and P. A. Witherspoon, A study of two-phase concurrent flow of steam and water in an unconsolidated porous medium. In *Heat Transfer in Porous Media and Particulate Flows*, HTD Vol. 46, *Proceedings of the 23rd ASME/AIChE National Heat Transfer Conf.*, Denver, 4–7 August, pp. 135–143 (1985).
18. M. Th. van Genuchten, A closed-form equation for predicting the hydraulic conductivity of unsaturated soils, *Soil Sci. Soc. Am. J.* **44**, 892–898 (1980).
19. K. Pruess and J. S. Y. Wang, TOUGH—a numerical model for nonisothermal unsaturated flow to study waste canister heating effects. In *Scientific Basis for Nuclear Waste Management* (Edited by G. L. McVay), Vol. 26, *Materials Research Society Symposia Proceedings*, pp. 1031–1038. North Holland, New York (1984).
20. K. Pruess, TOUGH User's Guide, Rep. NUREG/CR-4645, Nuclear Regulatory Commission, Washington, D.C. (1987).
21. C. Doughty and K. Pruess, Numerical modeling of a porous heat pipe: comparison with a semianalytical solution. In Earth Sciences Division Annual Report 1986, Rep. LBL-22090, Lawrence Berkeley Laboratory, Berkeley, California (1987).
22. K. S. Udell and J. S. Fitch, Heat and mass transfer in capillary porous media considering evaporation, condensation, and noncondensible gas effects. In *Heat Transfer in Porous Media and Particulate Flows*, HTD Vol. 46, *Proceedings of the 23rd ASME/AIChE National Heat Transfer Conf.*, Denver, 4–7 August (1985).
23. J. S. Fitch and K. S. Udell, Limits of multiphase heat and mass transfer in porous media, 86-HT-33, presented at the 4th AIAA/ASME Thermophysics and Heat Transfer Conf., Boston, 2–4 June (1986).

APPENDIX: SATURATION VARIATION IN THE HEAT PIPE REGION

To determine $S(r)$ in the heat-pipe region $r_i \leqslant r \leqslant r_o$, we begin with Darcy's law, modified for two-phase flow

$$\dot{m}_l = -\frac{k k_{rl}}{\nu_l}\frac{dP_l}{dr} \tag{A1}$$

$$\dot{m}_v = -\frac{k k_{rv}}{\nu_v}\frac{dP_v}{dr} \tag{A2}$$

where the subscripts v and l refer to vapor and liquid phases, respectively, $\dot{m}$ is mass flow rate per unit area, k is absolute permeability, k_r is the relative permeability of each phase, and ν is kinematic viscosity. Liquid pressure is less than vapor pressure because of the addition of the (negative) capillary pressure, P_{cap}

$$P_l = P_v + P_{cap} \tag{A3}$$

so we may write

$$\frac{dP_{cap}}{dr} = \frac{dP_l}{dr} - \frac{dP_v}{dr}. \tag{A4}$$

Under steady state conditions, liquid and vapor flows are equal in magnitude and opposite in direction

$$\dot{m}_l + \dot{m}_v = 0. \tag{A5}$$

For nuclear waste isolation, heat fluxes are relatively small, so that temperature and pressure gradients in the heat-pipe region are also small, and conductive heat flow there can be neglected. As a consequence, evaporation and condensation take place only at the hot and cold ends, respectively, of the heat pipe. The convective heat flux, q, is given by

$$q = \dot{m}_v h_{vl} \tag{A6}$$

where h_{vl} is the latent enthalpy of vaporization of the liquid. For linear geometry, q is a constant, but for radial geometry q is a function of r, given by

$$q = \frac{Q}{2\pi r} \tag{A7}$$

where Q is the constant heat source strength.

Substituting equations (A1), (A2) and (A5)–(A7) into equation (A4) gives

$$\frac{dP_{cap}}{dr} = \frac{Q}{2\pi r k h_{vl}}\left(\frac{\nu_v}{k_{rv}} + \frac{\nu_l}{k_{rl}}\right). \tag{A8}$$

Following Udell [8], we rewrite equation (A8) in non-dimensional form as

$$\frac{df}{d\delta} = -\omega\left(\frac{1}{k_{rv}} + \frac{\beta}{k_{rl}}\right) \tag{A9}$$

where

$$f = \frac{P_{cap}}{P_{c0}} \tag{A10}$$

$$\delta = \frac{r_o}{P_{c0}}(\rho_l - \rho_v) g \ln(r_o/r) \tag{A11}$$

$$\omega = \frac{Q\nu_v}{2\pi r_o k h_{vl}(\rho_l - \rho_v) g} \tag{A12}$$

$$\beta = \frac{\nu_l}{\nu_v}. \tag{A13}$$

Here P_{c0} is a (negative) reference pressure for a particular capillary pressure function, ρ is density, and g is gravitational acceleration. Equations (A9)–(A13) are identical to those for the linear heat pipe [8], except for the definitions of δ, where $r_o \ln(r_o/r)$ replaces the linear coordinate x, and ω, where $Q/2\pi r_o$ replaces the constant linear heat flux q. The non-dimensional parameter ω, giving the ratio of the vapor pressure gradient at $k_{rv} = 1$ to the buoyancy pressure gradient, provides a measure of the importance of gravity. For linear-geometry studies considering top, bottom, and horizontal heating, Udell [8] has shown that for values of $\omega > 10$ gravity is negligible. The results further suggest that gravity has only a modest effect for $\omega > 1$.

Equation (A9) describes the variation of non-dimensional capillary pressure f with non-dimensional radial distance δ. Since we want an expression for the variation of saturation S with δ, we need to write equation (A9) in terms of S. The relative permeabilities, k_{rv} and k_{rl}, and the non-dimensional capillary pressure, f, are all assumed to be single-valued (non-hysteretic) functions of S only, so $df/d\delta$ may be written as

$$\frac{df}{d\delta} = \frac{df}{dS}\cdot\frac{dS}{d\delta} = f'\cdot\frac{dS}{d\delta} \tag{A14}$$

where the notation $f' = df/dS$ is used. Hence equation (A9) may be written as

$$\frac{dS}{d\delta} = \frac{\omega\left(\frac{1}{k_{rv}} + \frac{\beta}{k_{rl}}\right)}{-f'}. \tag{A15}$$

Equation (A15) gives the fundamental relationship between scaled saturation S and non-dimensional length δ for the steady state of a heat pipe in one-dimensional radial geometry.

SOLUTION SEMI-ANALYTIQUE POUR LES EFFETS CALODUCS PRES DES CONTENEURS DE DECHETS NUCLEAIRES ENFOUIS DANS UN MILIEU GEOLOGIQUE PARTIELLEMENT SATURE

Résumé—Une source de chaleur intense, telle qu'un conteneur de déchets nucléaire, dans un milieu perméable partiellement saturé peut donner lieu au développement d'un caloduc. On analyse une version simplifiée de ce problème qui a une solution permanente, pour une géométrie radiale. La solution est obtenue sous forme semi-analytique et elle est comparée à la solution analogue pour un caloduc linéaire. Des applications diverses sont présentées pour des milieux poreux et aussi bien que poreux-fractués, avec différentes propriétés hydrologiques. Les paramètres déterminant la longueur du caloduc et la question de l'assèchement au voisinage de la masse sont discutés. La solution semi-analytique est vérifiée par simulation numérique qui montre comment se fait l'évolution depuis les conditions initiales uniformes jusqu'à l'éventuel état stationnaire.

EINE HALBANALYTISCHE LÖSUNG FÜR WÄRMEROHREFFEKTE IN DER NÄHE VON HOCHRADIOAKTIVEN ABFALLBEHÄLTERN, EINGEBRACHT IN TEILWEISE GESÄTTIGTE GEOLOGISCHE MEDIEN

Zusammenfassung—Das Einbringen einer starken Wärmequelle, wie z. B. eines Behälters mit hochradioaktivem Abfall, in ein teilweise gesättigtes durchlässiges Medium gibt Anlaß für die Ausbildung eines Wärmerohres. In der vorliegenden Arbeit wird eine vereinfachte Version dieses Problems mit einer stationären Lösung bei radialer Geometrie analysiert. Die Lösung erhält man in halbanalytischer Form; sie wird mit der analogen Lösung für ein geradliniges Wärmerohr verglichen. Verschiedene Anwendungen werden vorgestellt—sowohl für poröse als auch für gebrochen poröse Medien mit verschiedenen hydrologischen Eigenschaften. Die Parameter zur Bestimmung der Wärmerohrlänge und die Frage, ob die Umgebung der Wärmequelle austrocknet, werden erörtert. Die halbanalytische Lösung wird durch numerische Simulationen überprüft, welche die transiente Entwicklung von einheitlichen Ausgangs-Zuständen zu möglichen stationären End-Zuständen zeigen.

ПОЛУАНАЛИТИЧЕСКОЕ РЕШЕНИЕ ЗАДАЧИ ОБ ЭФФЕКТАХ ТЕПЛОВОЙ ТРУБЫ ВБЛИЗИ КОНТЕЙНЕРОВ С ВЫСОКОРАДИОАКТИВНЫМИ ЯДЕРНЫМИ ОТХОДАМИ, ЗАХОРОНЕННЫМИ В ЧАСТИЧНО НАСЫЩЕННЫХ ЖИДКОСТЬЮ ГЕОЛОГИЧЕСКИХ СРЕДАХ

Аннотация—Помещение такого мощного источника тепла, каким является контейнер с высокорадиоактивными ядерными отходами, в частично насыщенную жидкостью проницаемую среду приводит к образованию своего рода тепловой трубы. В данной работе анализируется упрощенный вариант такой задачи, которая имеет стационарное решение для радиальной геометрии тепловой трубы. Решение получено в полуаналитическом виде и дано сравнение с аналогичным решением для тепловой трубы линейной формы. Показаны различные применения такого решения как для пористых, так и для трещиновато-пористых сред с различными гидрологическими свойствами. Рассматриваются параметры, которые определяют длину тепловой трубы, а также вопрос о том, влияет ли источник тепла на высыхание окружающего грунта. Полуаналитическое решение проверяется с помощью численного моделирования, которое указывает на переход от равномерных начальных однородных условий к конечному стационарному состоянию.